RSC Advances

ROYAL SOCIETY OF CHEMISTRY

www.rsc.org/advances

Environmental performances of hydrochar-derived magnetic carbon composite affected by its carbonaceous precursor

Xiangdong Zhu, Feng Qian, Yuchen Liu, Shicheng Zhang*, Jianmin Chen

Shanghai Key Laboratory of Atmospheric Particle Pollution and Prevention (LAP^3), Department of Environmental Science and Engineering, Fudan University, Shanghai 200433, China

* Corresponding author.

Tel/fax: +86-21-65642297;

E-mail address: zhangsc@fudan.edu.cn.

The effects of hydrochar properties on the environmental performances of its derived magnetic carbon composite have been overlooked. In the present work, various hydrochar (produced from different hydrothermal carbonization temperature, 160-300°C) were selected as the carbonaceous precursors. Then, magnetic carbon composites were fabricated by simultaneously carbonizing hydrochar, $ZnCl_2$ and $FeCl_3$ (namely simultaneous activation and magnetization). It was observed that a magnetic carbon composite with high porosity, acid resistance and adsorption capacity for roxarsone, and low graphitization degree was prepared from a hydrochar with low hydrothermal carbonization temperature. More importantly, strong linear correlations were obtained between hydrochar properties (recalcitrance index, H/C and O/C atomic ratios) and the environmental performances of its derived magnetic carbon composites (porosity, acid resistance, degree of graphitization, and adsorption capacity for roxarsone). The adsorption of ROX molecules onto the as-prepared magnetic carbon composite were mainly regulated by the pores of materials under certain solution pH. This work provides novel insights into the role of hydrochar properties in determining the environmental performances of its derived magnetic carbon composite.

1 Introduction

In the past few years, magnetic carbon composites have been received much attention due to their facile separation property and high adsorption capacity for pollutants removal.[1, 2] Biomass and its derived char, an abundant and sustainable carbonaceous precursor, have been considered as a renewable material for the preparation of advanced magnetic carbon composites.[3-5]

Recently, hydrochar (a solid product from the hydrothermal carbonization (HTC) of biomass) exhibits an excellent carbonaceous precursor for the fabrication of advanced carbon composite, due to its higher carbon content and lower ash content than raw biomass.[6-9] Given the low porosity of hydrochar (< 10 m^2/g), considerable progress have been made in the optimization of external conditions for hydrochar activation, such as activation temperature and activator loading and kind, in order to obtain a magnetic carbon composite with high porosity.[7, 10-13]

In the current literatures, it has been well reported that the properties of hydrochar were greatly affected by its production conditions. For example, the carbonization degree of hydrochar increases with increasing HTC temperature.[14-16] Very recently, hydrochar was activated to prepare hydrochar-based porous carbon (namely activated carbon) by $ZnCl_2$ activator, and the correlations between the hydrochar properties and the porosity of hydrochar-based porous carbon (namely activated carbon) were also observed by our group.[17]

Unlike the porous carbon, magnetic carbon composite should pay more attention to its acid resistance and graphitization degree, due to addition of iron salt (precursor of magnetic medium).[18] The graphitization degree and acid resistance of magnetic carbon composite were

closely related to its adsorption capacity and practical reuse. In addition, due to catalysis effect of iron salt, the porosity of magnetic carbon composite would be changed. Therefore, it is of great importance to explore the roles of hydrochar properties (namely internal activation conditions) in the environmental performances (porosity, acid resistance, graphitization degree and adsorption capacity) of magnetic carbon composite.

Roxarsone (4-hydroxy-3-nitrophenylarsonic acid, ROX) was selected as a model adsorbate in the examination of the adsorption characteristics of as-prepared magnetic carbon composites. ROX is an organoarsenic additive and has been widely used as herbicides, pesticides and antimicrobial growth promoters.[19, 20] Most of ROX molecules were excreted via manure with unchanged structures. It has been reported that arsenic was found within manure in China with concentrations of 89.3 mg/kg.[21] The ROX molecule possesses a low toxicity, but inorganic arsenic species, such as arsenite and arsenate, may be produced from the biogeochemical degradation of ROX.[14, 15] This may result in potential risks to both the environment and human health.

Although carbonaceous materials and iron oxides exhibited great performance for organoarsenic adsorption,[22-25] the disadvantage of hard collection and high iron leaching hindered their practical application. However, magnetic carbon composites were versatile adsorbents and could provide both adsorption sites and a facile collection characteristic. Therefore, there is a need to investigate ROX adsorption onto such adsorbents from water bodies in the exploration of a facile and efficient adsorption process.

The main objective of this paper was the determination of correlations between the characteristics of hydrochar precursors and the environmental performances of their derived magnetic carbon composites. To achieve this purpose, hydrochar was produced at different HTC temperatures due to the fact that the properties (such as thermal stability) of hydrochar were more sensitive to HTC temperature than HTC retention time and feedstock type (evaluated by a heterogeneity index). Then, the resulting hydrochar materials were further activated to prepare magnetic carbon composites through simultaneous activation and magnetization method. The hydrochar materials were quantitatively characterized with thermal recalcitrance and atomic ratios, and the resultant magnetic carbon composites were quantitatively characterized with porosity, acid resistance, degree of graphitization, and ROX adsorption capacity. The mechanism for ROX adsorption onto an as-prepared magnetic carbon composite was also examined.

2 Methods

Hydrochar preparation

Sawdust, obtained from a furniture factory, was hydrothermally transformed for the preparation of hydrochar. The cellulose, hemicellulose and lignin contents (analytical method: GB/T2677.10-1995 NREL and GBT10337-2008 NREL) of the raw material were 39.9, 19.4 and 17.7 %, respectively. For each hydrothermal reaction, 15 g of sawdust and 150 g of deionized water were placed in an autoclave (250 mL) and sealed. The reactor heated up at different temperatures (160 to 300 °C) with a constant retention time of 60 min and at an autogenic pressure of 0-8 Mpa. The variations of the HTC temperatures and pressures as functions of

reaction time are presented in Fig. S1.

The collected solid material was thoroughly washed three times with 1M hydrochloride (HCl) to reduce the inorganic salts and successively washed three times with deionized water. The resulted hydrochar was denoted as *H-T*, where *H* refers to hydrochar and *T* is HTC temperature in °C (i.e., 160, 200, 240, 270 or 300).

Simultaneous activation and magnetization process of hydrochar

The hydrochar-derived magnetic carbon composites were prepared by using the simultaneous activation and magnetization method, as shown in following suggestion. Briefly, 2 g of $FeCl_3 \cdot 6H_2O$, 8 g of $ZnCl_2$ and 8 g of hydrochar were mixed in 50 mL deionized water. The $FeCl_3$ and $ZnCl_2$ were of analytical reagent (Sinopharm, China). This mixture were stirred for 24 h and then dried at 80 °C for 4 h in air. Subsequently, these dried mixtures were heated at 600 °C for 90 min under a nitrogen gas (N_2) flow of 1 L/min. The concentration of the activator ($ZnCl_2$) and the activation temperature were used according with previous work.[13] The crude magnetic carbon composite was successively washed with 0.1 M HCl, ethanol and deionized water. The resulted magnetic carbon composite was denoted as *MC-T*, where *MC* refers to the magnetic carbon composite, *T* is the production temperature of the hydrochar (i.e., the precursor of magnetic carbon composite) in °C (i.e., 160, 200, 240, 270 or 300).

Characterizations of hydrochar and hydrochar-derived magnetic carbon composite

The hydrochar samples were characterized by thermogravimetry (TG) and derivative thermogravimetry (DTG), with heating conditions from room temperature to 1000 °C under an

air atmosphere at a rate of 20 °C/min. The novel recalcitrance index for the hydrochar samples, R_{50}, was also quantitatively calculated as:

$$R_{50} = \frac{T_{50,\,\text{hydrochar}}}{T_{50,\,\text{graphite}}}$$

where $T_{50,\,\text{hydrochar}}$ and $T_{50,\,\text{graphite}}$ were the temperature values corresponding to 50 % weight loss by oxidation and volatilization of the hydrochar sample and graphite, respectively. Values for $T_{50,\,\text{hydrochar}}$ and $T_{50,\,\text{graphite}}$ were obtained directly from TG curves that had been corrected for water and ash content. Graphite was a reference substance and purchased from Alfa Aesar (purity 99.9995 %, 100 mesh). More details on the calculation of the R_{50} index were provided in Harvey et al..[26]

The elemental compositions of samples were analyzed with an elemental analyzer (Vario EL III). The combustion temperature was 950 °C. The functional groups of the samples were examined using Fourier transform infrared spectroscopy (FTIR, Nexus470). FTIR spectra of samples were collected at a resolution of 2 cm^{-1}, and the wavenumber ranged from 4000 to 400 cm^{-1}. The phase structure was characterized with powder X-ray diffraction (XRD). The scan rate and step size for the XRD analysis was 4 °/min and 0.02º in 2θ. Raman spectra were obtained from the LabRam-1B spectrometer with He-Ne laser operating at a wavelength of 514 nm, and the curve fitting were performed with the combination of Gaussian line shapes that gave the minimum fitting error.

Transmission electron microscopy (TEM) images were obtained on a TECNAI-G2 (FEI) transmission electron microscope at an accelerating voltage of 200 kV. Samples dispersed at an

appropriate concentration in ethanol were cast onto a carbon-coated Cu double-grid. Energy-dispersive X-ray (EDX) spectra were measured on the TEM instrument with an EDX spectrometer.

The pore structure characteristics of samples were determined on a Tristar 3000 by nitrogen adsorption at -196 °C. The surface area was calculated from the isotherm using the Brunauer-Emmett-Teller (BET) equation. The volume and surface area of the micropores were obtained with the t-plot method. Magnetic measurement was carried out at room temperature by a vibrating sample magnetometer (VSM, MPMS, SQUID) with a maximum magnetic field of ± 20000 Oe.

The acid resistance (Fe leaching) was performed at 2000 mg/L magnetic carbon composite with 24 h contact time at room temperature under pH 2.0 and 3.0. Additionally, in order to calculate the content of iron oxide (Fe_2O_3) particles within the as-prepared magnetic carbon composites, the extracted Fe element was determined by inductively coupled plasma (ICP, P-4010), following the acid digestion (HCl-HNO_3) procedure. The experiments of Fe leaching and Fe_2O_3 content were performed in duplicate.

Adsorption of roxarsone

Adsorption kinetics and isotherms were performed to examine the adsorption reactions of ROX. Analytical grade ROX was purchased from J&K Chemical Ltd. To examine the ROX adsorption kinetics, the initial concentration of ROX was set at 400 mg/L, and samples were taken from 0 to 24 h. Adsorption isotherms were run with six points (50 to 500 mg/L) for all

magnetic carbon composites, the adsorption equilibrium time was 24 h. To initiate the experiments of adsorption kinetics and equilibrium, 0.02 g of adsorbent were added to a 60 mL glass vial, followed by a stock solution of ROX (500 mg/L, prepared in water) and a desired volume of deionized water (pH 6.8). These vials contained 50 mL of solution and were stirred at 120 rpm at 25 °C. All adsorption experiments were performed in triplicate.

After adsorption equilibrium, the supernatant was separated from the magnetic carbon composite by filtration using a 0.22 μm polytetrafluoroethylene (PTFE) membrane filter. The concentrations of ROX were determined using an ultraviolet-visible (UV-vis) spectrophotometer (HACH, DR6000) at a wavelength of 268 nm.

3 Results and discussion

Chemical characteristics of hydrochar

The main physicochemical properties for the hydrochar samples are shown in Table 1. As expected, the yields and the H/C, O/C atomic ratios of the hydrochar samples (except for the atomic ratios of *HC-300* sample) decreased gradually with increasing HTC temperature, due to the increasing carbonization extent of raw sawdust. It has been well documented that the H/C and O/C atomic ratios can be used to estimate the aromaticity and polarity of carbonaceous material, respectively.[14, 15] Lower H/C and O/C atomic ratios indicated that the hydrochar sample contained more aromatic carbon and became less hydrophilic. Thus, hydrochar samples with high aromaticity and low polarity were observed at higher HTC temperatures. The variation of aromaticity of the hydrochar sample was also confirmed by the FTIR spectra, as indicated by an

increased intensity in the aromatic C=C (1616 cm^{-1}) character with HTC temperature (see Fig. S2). A more detailed interpretation for the evolution of FTIR spectra is provided in Fig. S2.

The TG thermograms in Fig. 1a indicate that there was a continuous increase in the T_{50} value when the HTC temperature was increased from 160 to 300 °C, due to the gradual loss of labile organic matter and the production of more stable matter.[27] Accordingly, the R_{50} value of the hydrochar samples increased with increasing HTC temperatures. Hence, the hydrochar materials became more thermally recalcitrant (Table 1), which was confirmed by the DTG thermograms (Fig. 1b). More details on the interpretation of the DTG curves for hydrochar is provided in Text S1. Harvey reported that the thermal recalcitrance of carbonaceous material was mainly driven by its degree of aromatization.[26] This was also supported by a strong negative correlation between the H/C atomic ratio and the R_{50} value of hydrochar, as indicated by Fig. 1c. Overall, the characteristics related to the elemental composition of hydrochar samples were in good agreement with data obtained through the TG characterization techniques.

Porous textural characteristics of hydrochar-derived magnetic carbon composite

As shown in Table 2, increased production temperatures of hydrochar had a positive effect on the yield of the magnetic carbon composite, suggesting that the environmental performance of the resultant magnetic carbon composite would be affected by the type of hydrochar. Interestingly, strong correlations were obtained between the yields of the magnetic carbon composite and the TG and elemental characteristics of the hydrochar precursor, including the R_{50} index and the H/C and O/C atomic ratios (Fig. S3). Thus, under a given activation condition, the

187 yield of hydrochar-derived magnetic carbon composites could be forecasted accurately by the
188 properties of their precursors.

189 The N_2 adsorption isotherms and pore size distribution of different hydrochar-derived
190 magnetic carbon composites are shown in Fig. S4. Obviously, the first three magnetic carbon
191 composites (*MC-160*, *MC-200* and *MC-240* samples) exhibited a type I isotherm, which was
192 typical of microporous materials. And the *MC-270* and *MC-300* samples exhibited a type IV
193 isotherm, indicating the development of mesoporous. The majority of pores in the as-prepared
194 magnetic carbon composites possessed diameter of less than 2 nm, which further confirmed the
195 microporous structure of the resultant materials. However, there was a continuous downward
196 shift in the N_2 adsorption of the magnetic carbon composites with increasing production
197 temperature of the hydrochar precursor. The BET surface area (S_{BET}), micropore surface area
198 (S_{mic}), total pore volume (V_t) and micropore volume (V_{mic}) of the magnetic carbon composites
199 decreased with increasing production temperature of the hydrochar (see Table 2), suggesting that
200 the production temperature of the hydrochar strongly affected the porosity of its derived
201 magnetic carbon composites. This trend can be attributed to the higher carbonization extent that
202 was developed to produce micoropores when a low-temperature hydrochar served as precursor.
203 This explanation was consistent with the increase in the yield of magnetic carbon composite as
204 the production temperature of the hydrochar increased (Table 2). In addition, the proportion of
205 microporosity (indicated by S_{mic}/S_{BET} and V_{mic}/V_t ratios) remained unchanged with the production
206 temperature of the hydrochar (except for the *MC-270* sample).

The correlations between the porosity of magnetic carbon composites and the properties of their hydrochar precursors, including the R_{50} index, the H/C and O/C atomic ratios, were also investigated. As shown in Table S1, the porosity (S_{BET}, S_{mic}, V_t and V_{mic}) of the magnetic carbon composites was negatively correlated with the R_{50} index of the hydrochar precursor and positively correlated with the H/C and O/C atomic ratios of the hydrochar. This indicated that the chemical activation reaction of hydrochar material by $ZnCl_2$ and $FeCl_3$ was resisted by the aromatic carbon of thermal recalcitrance. Hence, the characteristics of a hydrochar were good indicators of porosity for its derived magnetic carbon composite.

Morphology, magnetic properties and acid resistance of magnetic carbon composite

The TEM image of typical hydrochar-derived magnetic carbon composite is shown in Fig. 2, the sample was mainly composed of multi-layer carbon sheet. The distributions of C, Fe, and O elements have been investigated by the corresponding elemental mapping images (EDX analysis). The central region of particle appeared bright due to the presence of higher atomic weight Fe atoms.[28] It can be seen that Fe and O element was uniformly distributed in the carbon surfaces. Therefore, it can be assumed that some Fe-O moieties were grown on the carbon surface.

As shown in Fig. S5, the crystalline phases within the as-prepared magnetic carbon composites were iron oxides (γ-Fe_2O_3 and α-Fe_2O_3) via the thermal decomposition of $FeCl_3$,[13, 29, 30] partly confirmed the results of Fe and O elemental mapping. The peaks at 2θ of 30.0º, 35.3º, 42.9º, 53.5º, 56.9º and 62.4º were assigned to γ-Fe_2O_3. Moreover, the weak peak at 2θ of 36.5º

was related to presence of α-Fe_2O_3. The characteristics of the XRD peaks showed no apparent change on the basis of their type and intensity.

Obviously, the γ-Fe_2O_3 particles were the main magnetic composition. As shown in Fig. S6a, weak magnetic hysteresis loop were also observed. The saturation magnetization of the as-prepared magnetic carbon composites ranged from 13.6 to 16.3 emu/g, due to their different contents of Fe_2O_3 particles (Table S2). This magnetic characteristic ensured that the as-prepared magnetic carbon composites were suitable for the separation of particles from the aqueous solution, as indicated by the Fig. S6.[31]

Table S2 shows the effect of the hydrochar type on the Fe leaching concentrations under acidic conditions (pH values of 2.0 and 3.0). Obviously, a low-temperature hydrochar-derived magnetic carbon composites exhibited strong acid resistance, due to the lower dissolution capability of Fe_2O_3 particles under acidic conditions. As shown in Fig. S7, the Fe leaching concentrations under acidic conditions were well controlled by the porosity of the magnetic carbon composites, especially under pH 2.0 conditions, indicating that high porosity magnetic carbon composites possessed strong acid resistance. This can be attributed to the Fe_2O_3 particles derived from a high-porosity magnetic carbon composite being well wrapped by its carbon matrix, due to the strong interaction between the Fe_2O_3 particles and the carbon matrix.

The above porosity analysis showed the porosity of magnetic carbon composites was well correlated with the properties of hydrochar. Hence, it was expected that Fe leaching concentrations of magnetic carbon composites also could be further linked with the properties of

hydrochar. As anticipated, strong correlations were observed between the Fe leaching concentrations of the magnetic carbon composites and the properties (the R_{50} index, the H/C and O/C atomic ratios) of the hydrochar precursors (Fig. 3). These correlations suggested that, acid resistance of the as-prepared magnetic carbon composites were also regulated by the properties of their precursors. It should be noted that a low-temperature hydrochar-derived magnetic carbon composite not only had high porosity, but also exhibited high acid resistance, indicating preferable practical application for pollutant removal.

FTIR and Raman analysis of magnetic carbon composite

As shown in Fig. 4a, the FTIR spectra of the as-prepared magnetic carbon composites showed similar characteristics and weak differences in the adsorption intensities and shifts due to different precursors. The adsorption of the C=C vibration in the aromatics group at 1596 cm^{-1} for the *MC-160, 200* and *240* samples were shifted to lower wave numbers of 1537 and 1561 cm^{-1} for *MC-270* and *MC-300* products, respectively, due to the formation of weaker C-O-Fe bonds. The band assigned to the C-O vibration in ester or ether also exhibited a similar observation, also confirming the formation of C-O-Fe bonds.[32] The bands at 658 and 565 cm^{-1} (Fe-O stretching) confirmed the formation of γ-Fe_2O_3 on the composites.[33] It should be noted that the high-temperature hydrochar-derived magnetic carbon composites had higher FTIR adsorption intensities for the above two bands, possibly due to a reduced coating impact of the carbon matrix. These results further confirmed that a high-temperature hydrochar-derived magnetic carbon composite possessed weak acid resistance.

As shown in Fig. 4b, the Raman spectra of the as-prepared magnetic carbon composites consisted of two prominent characteristic peaks, namely the D band assigned to the presence of defects at ~ 1332 cm^{-1} and the G band for the graphitic sheet at ~ 1590 cm^{-1}.[33, 34] It was interesting to note that the G band in all the as-prepared magnetic carbon composites was located at a higher frequency than in graphite (1590 versus 1580 cm^{-1}),[35] indicating an interaction, such as charge transfer, between graphite and Fe_2O_3 particles.[32] Because of the coating effect of the carbon matrix, the band assigned to the Fe_2O_3 (~ 500 cm^{-1}) in the Raman spectra were not observed, confirming the strong acid resistance of the as-prepared magnetic carbon composites.

Typically, the relative intensity ratio of the D band to the G band (I_D/I_G) provides the degree of graphitization of the as-prepared products.[34] Obviously, high-temperature hydrochar-derived magnetic carbon composites possessed the lower I_D/I_G value, revealing that increasing the hydrochar production temperature substantially increased the graphitization degree of the final activation material. Hence, the graphitization degree of hydrochar-derived magnetic carbon composites was also regulated by their precursors.

To elucidate the correlations between the I_D/I_G value of magnetic carbon composites and their precursors, the I_D/I_G values were also plotted versus the R_{50} index, H/C and O/C atomic ratios, as shown in Fig. 5. Interestingly, a linear decrease in the I_D/I_G values as a function of the R_{50} index was observed, whereas linear increases in the I_D/I_G value as functions of the H/C and O/C atomic ratios were obtained, suggesting that a hydrochar-derived magnetic carbon composite with a low I_D/I_G value resulted from a precursor with a high degree of carbonization (indicated by high

thermal recalcitrance, high aromaticity and low polarity). Hence, under a given activation condition, the graphitization degree of hydrochar-derived magnetic carbon composites could also be predicted based on the properties of the precursor material.

Adsorption of roxarsone onto magnetic carbon composite

The pseudo-second-order kinetics and Langmuir equation were used to fit the adsorption kinetics and isotherms of ROX onto the as-prepared magnetic carbon composites, respectively, as shown in Fig. S8 and S9. A more detailed interpretation for the ROX adsorption kinetics and isotherms is provided in Text S2. The fitted data are shown in Table 3. The as-prepared magnetic carbon composites exhibited fast adsorption rates and large adsorption capacities for ROX removal from aqueous solutions, indicating that these materials could be excellent candidates for the design of a separable material for ROX removal.

It has been well documented that the high porosity of porous carbon material can enhance the adsorption of organic pollutants, due to the pronounced pore filling effect.[36] As shown in Fig. S10, strong positive correlations between the ROX adsorption uptake at equilibrium (q_e, obtained from the pseudo-second-order kinetics equation) and the porosity of as-prepared magnetic carbon composites were observed. Similar trends were observed between the ROX maximum adsorption capacity (q_m, obtained from the Langmuir equation) and the porosity of the as-prepared magnetic carbon composites (see Fig. S11), due to the effect of pore filling. Although it has been reported that ROX adsorption onto an iron oxide composite were partly driven by surface complex interaction, including As (V) moiety of the ROX molecule interacting

with the surface of iron oxide.[37] However, it should be emphasized that the Fe_2O_3 particles within as-prepared magnetic carbon composites were well wrapped by carbon matrix. Therefore, the ROX adsorption mechanism onto the as-prepared magnetic carbon composites was mainly dominated by the effect of pore filling under certain solution pH, as further indicated by Fig. S10 and S11.

Fig. 6 presented the TEM-EDX elemental mappings of C, As, Fe, and O element for the hydrochar-derived magnetic carbon composite adsorbed with ROX molecule, which indicated that As element (typical from the ROX molecule) were homogeneously adsorbed on the carbon surface. However, the Fe elements were concentrated on the central region. This was confirmed that the ROX adsorption onto the as-prepared magnetic carbon composites was mainly dominated by the carbon surface.

As suggested in Table S1, the porosity of hydrochar-derived magnetic carbon composites was notably correlated with the hydrochar properties. In order to determine a direct link between ROX adsorption characteristics *(q_e* and *q_m)* and hydrochar properties, the values of q_e and q_m were also plotted against the various properties of hydrochar, including the R_{50} index, H/C and O/C atomic ratios, as shown in Fig. 7 and Fig. S12. As expected, strong correlations between ROX adsorption characteristics and hydrochar properties were observed, and magnetic carbon composite derived from low temperature hydrochar sample exhibited high adsorption capacity for ROX removal. Hence, the adsorption performance of hydrochar-derived magnetic carbon composites was also greatly dependent on the properties of the precursor hydrochar.

4 Conclusions

Overall, the environmental performances of hydrochar-derived magnetic carbon composite, including porosity, acid resistance, degree of graphitization and adsorption capacity, was well correlated with the TG and elemental characteristics of their hydrochar precursor (produced from different temperature). A magnetic carbon composite with high porosity, high acid resistance and low graphitization degree was derived from a hydrochar with the characteristic of low aromaticity and thermal recalcitrance, and high polarity. In addition, the as-prepared magnetic carbon composite exhibited high potential for the removal of ROX and could be easily separated from the aqueous solution.

Acknowledgements

This research was supported by the National Natural Science Foundation of China (No. 21407027), National Key Technology Support Program (No. 2015BAD15B06), and Shanghai Talent Development Fund (No. 201414).

Electronic supplementary information (ESI) available.

References

1 B. Qiu, H. Gu, X. Yan, J. Guo, Y. Wang, D. Sun, Q. Wang, M. Khan, X. Zhang and B. L. Weeks, *J. Mater. Chem. A*, 2014, **2**, 17454-17462.

2 S. Zhang, M. Zeng, J. Li, J. Li, J. Xu and X. Wang, *J. Mater. Chem. A*, 2014, **2**, 4391-4397.

3 Z. H. Ruan, J. H. Wu, J. F. Huang, Z. T. Lin, Y. F. Li, Y. L. Liu, P. Y. Cao, Y. Fang and J. Xie, *J. Mater. Chem. A*, 2015, **3**, 4595-4603.

4 A. Jain, S. Jayaraman, R. Balasubramanian and M. Srinivasan, *J. Mater. Chem. A*, 2014, **2**, 520-528.

5 Y. L. Chen, S. Q. Chen, K. Tian, J. J. Chen and H. Jiang, *J. Mater. Chem. A*, 2015, DOI: 10.1039/C5TA01011J.

6 L. Dai, B. Wu, F. Tan, M. He, W. Wang, H. Qin, X. Tang, Q. Zhu, K. Pan and Q. Hu, *Bioresour. Technol.*, 2014, **161**, 327-332.

7 W. Hao, E. Bjorkman, M. Lilliestråle and N. Hedin, *Ind. Eng. Chem. Res.*, 2014, **53**, 15389-15397.

8 W. Hao, E. Björkman, Y. Yun, M. Lilliestråle and N. Hedin, *ChemSusChem*, 2014, **7**, 875-882.

9 M. Zhang, B. Gao, J. Fang, A. E. Creamer and J. L. Ullman, *RSC Adv.*, 2014, **4**, 28171-28175.

10 M. Sevilla, A. Fuertes and R. Mokaya, *Energ. Environ. Sci.*, 2011, **4**, 1400-1410.

11 A. Romero-Anaya, M. Ouzzine, M. Lillo-Ródenas and A. Linares-Solano, *Carbon*, 2014, **68**, 296-307.

12 X. Zhu, Y. Liu, C. Zhou, S. Zhang and J. Chen, *ACS Sustainable Chem. Eng.*, 2014, **2**, 969-977.

13 X. Zhu, Y. Liu, G. Luo, F. Qian, S. Zhang and J. Chen, *Environ. Sci. Technol.*, 2014, **58**, 5840-5848.

14 A. Budai, L. Wang, M. G. Gronli, L. T. Strand, M. J. Antal, S. Abiven, A. Dieguez-Alonso, A. Anca-Couce and D. P. Rasse, *J. Agric. Food Chem.*, 2014, **62**, 3791-3799.

15 X. Cao, K. S. Ro, J. A. Libra, C. I. Kammann, I. Lima, N. Berge, L. Li, Y. Li, N. Chen and J. Yang, *J. Agric. Food Chem.*, 2013, **61**, 9401-9411.

16 G. K. Parshetti, S. Chowdhury and R. Balasubramanian, *Bioresour. Technol.*, 2014, **161**, 310-319.

17 X. Zhu, Y. Liu, F. Qian, C. Zhou, S. Zhang and J. Chen, *ACS Sustainable Chem. Eng.*, 2015, DOI: 10.1021/acssuschemeng.5b00153.

18 X. Zhang, Y. Li, G. Li and C. Hu, *RSC Adv.*, 2015, **5**, 4984-4992.

19 X. D. Zhu, Y. J. Wang, C. Liu, W. X. Qin and D. M. Zhou, *Chemosphere*, 2014, **107**, 274-281.

20 M. Yoshinaga and B. P. Rosen, *Proc. Nati. Acad. Sci.*, 2014, **111**, 7701-7706.

21 L. Shi, W. Wang, S. Yuan and Z. Hu, *Environ. Sci. Technol.*, 2014, **48**, 7951-7958.

22 D. Arts, M. Abdus Sabur and H. A. Al-Abadleh, *J. Phys. Chem. A*, 2013, **117**, 2195-2204.

23 W. R. Chen and C. H. Huang, *J. Hazard. Mater.*, 2012, **227**, 378-385.

24 J. Hu, Z. Tong, Z. Hu, G. Chen and T. Chen, *J. Colloid Interf. Sci.*, 2012, **377**, 355-361.

25 S. Depalma, S. Cowen, T. Hoang and H. A. Al-Abadleh, *Environ. Sci. Technol.*, 2008, **42**, 1922-1927.

26 O. R. Harvey, L.-J. Kuo, A. R. Zimmerman, P. Louchouarn, J. E. Amonette and B. E. Herbert, *Environ. Sci. Technol.*, 2012, **46**, 1415-1421.

27 S. Kang, X. Li, J. Fan and J. Chang, *Ind. Eng. Chem. Res.*, 2012, **51**, 9023-9031.

28 L. Ling and W. X. Zhang, *J. Am. Chem. Soc.*, 2015, **137**, 2788-2791.

29 Y. Li, C. Zhu, T. Lu, Z. Guo, D. Zhang, J. Ma and S. Zhu, *Carbon*, 2013, **52**, 565-573.

30 Y. Zhai, Y. Dou, X. Liu, B. Tu and D. Zhao, *J. Mater. Chem.*, 2009, **19**, 3292-3300.

31 J. D. Xiao, L. G. Qiu, X. Jiang, Y. J. Zhu, S. Ye and X. Jiang, *Carbon*, 2013, **59**, 372-382.

32 J. Zhou, H. Song, L. Ma and X. Chen, *RSC Adv.*, 2011, **1**, 782-791.

33 A. P. Singh, M. Mishra, P. Sambyal, B. K. Gupta, B. P. Singh, A. Chandra and S. K. Dhawan, *J. Mater. Chem. A*, 2014, **2**, 3581-3593.

34 H. J. Lee, W. Cho, E. Lim and M. Oh, *Chem. Comm.*, 2014, **50**, 5476-5479.

35 M. Baikousi, A. B. Bourlinos, A. Douvalis, T. Bakas, D. F. Anagnostopoulos, J. i. Tuček, K. r. Šafářová, R. Zboril and M. A. Karakassides, *Langmuir*, 2012, **28**, 3918-3930.

36 M. Xie, W. Chen, Z. Xu, S. Zheng and D. Zhu, *Environ. Pollut.*, 2014, **186**, 187-194.

37 J. H. Kwon, L. D. Wilson and R. Sammynaiken, *Mater.*, 2014, **7**, 1880-1898.

Figure captions:

Fig. 1. Water and ash content-corrected TG (a) and DTG thermograms (b) of hydrochar samples produced under different HTC temperatures, and correlation between H/C atomic ratio and R_{50} index for hydrochar.

Fig. 2. The TEM image and elemental mapping spectra of C, Fe and O elements for the hydrochar-derived magnetic carbon composite (*MC-160*).

Fig. 3. Correlations between Fe leaching concentration of magnetic carbon composites and the hydrochar properties, including R_{50} index (a), H/C atomic ratio (b) and O/C atomic ratio of hydrochar.

Fig. 4. FTIR (a) and Raman (b) spectra of hydrochar-derived magnetic carbon composites.

Fig. 5. Correlations between I_D/I_G value of magnetic carbon composites and the hydrochar properties, including R_{50} index (a), H/C atomic ratio (b) and O/C atomic ratio of hydrochar.

Fig. 6. The TEM image and elemental mapping spectra of C, As, Fe and O elements for the hydrochar-derived magnetic carbon composite (*MC-160*) adsorbed with the ROX molecule.

Fig. 7. Correlations between q_m value (obtained from Langmuir equation) for ROX adsorption onto the as-prepared magnetic carbon composites and the hydrochar properties, including R_{50} index (a), H/C atomic ratio (b) and O/C atomic ratio (c) of hydrochar.

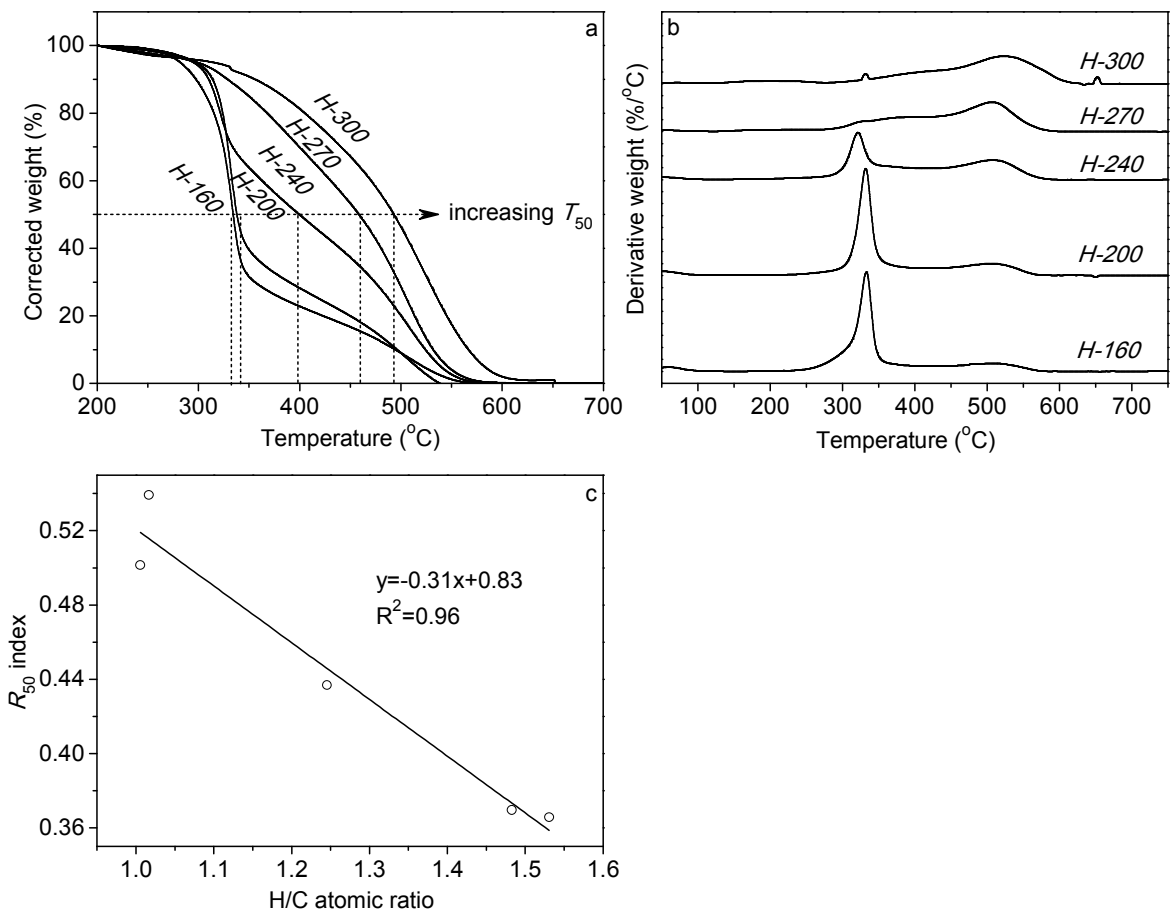

Fig. 1.

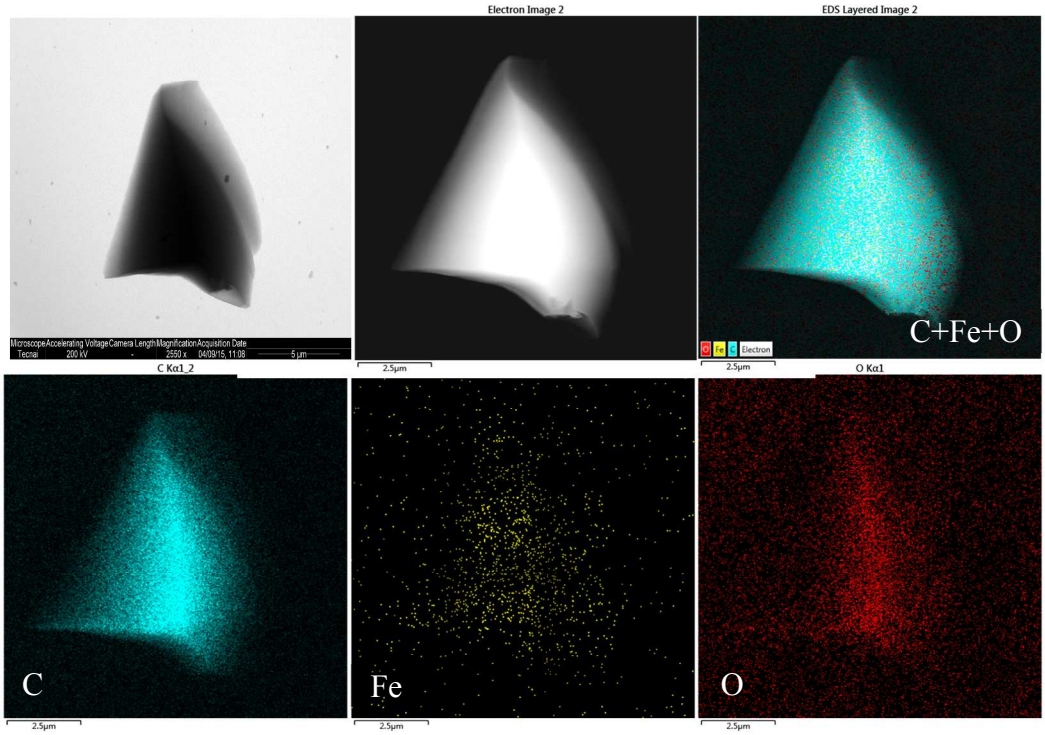

Fig. 2.

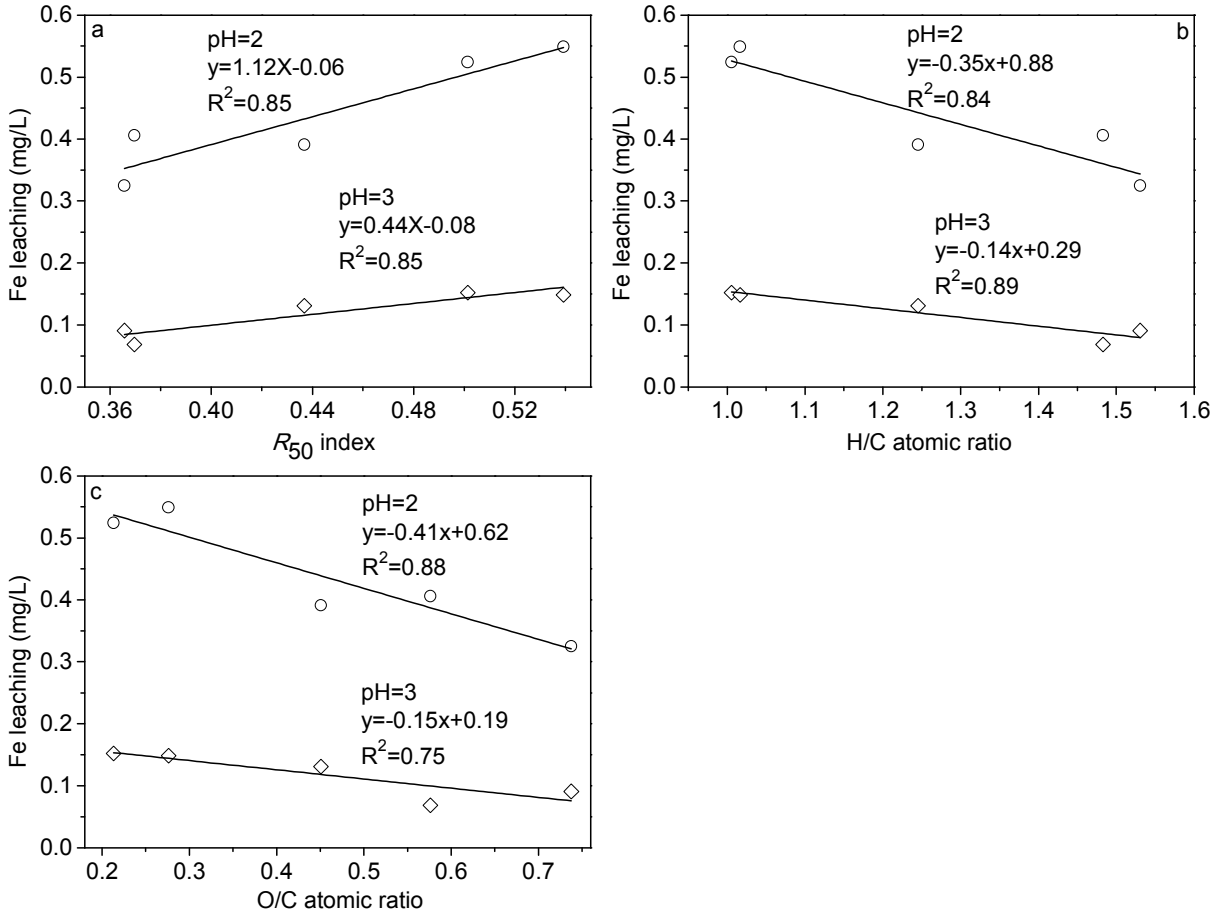

Fig. 3.

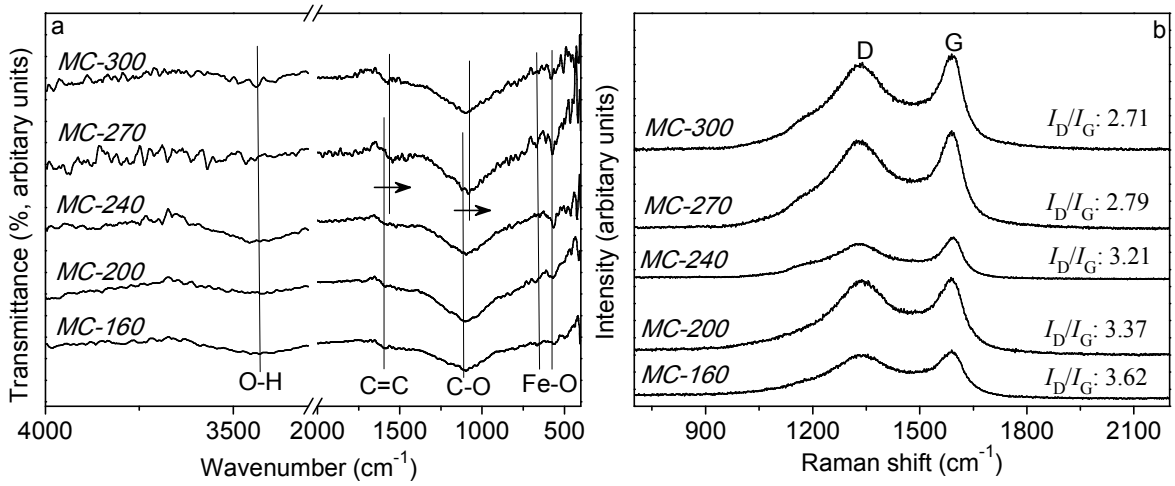

Fig. 4.

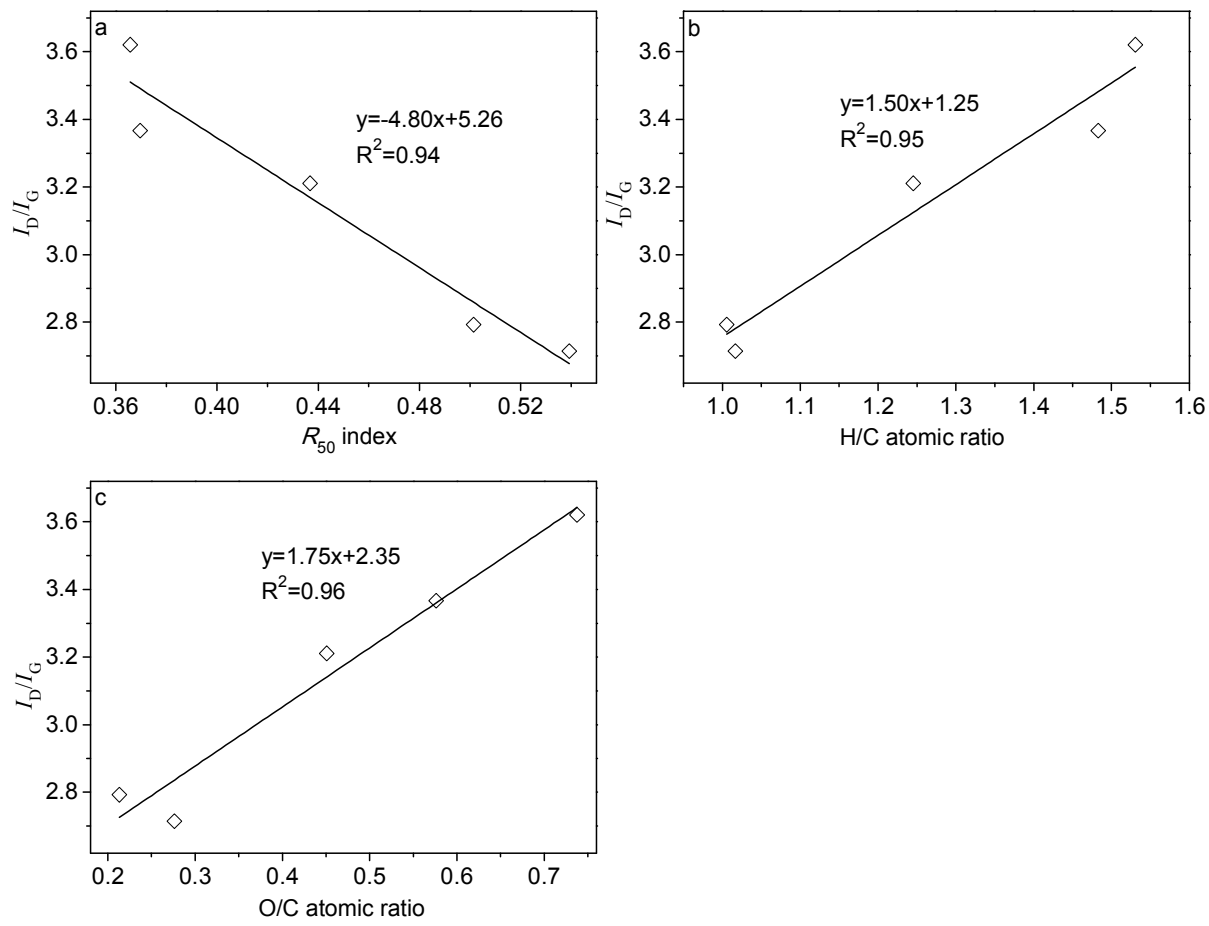

Fig. 5.

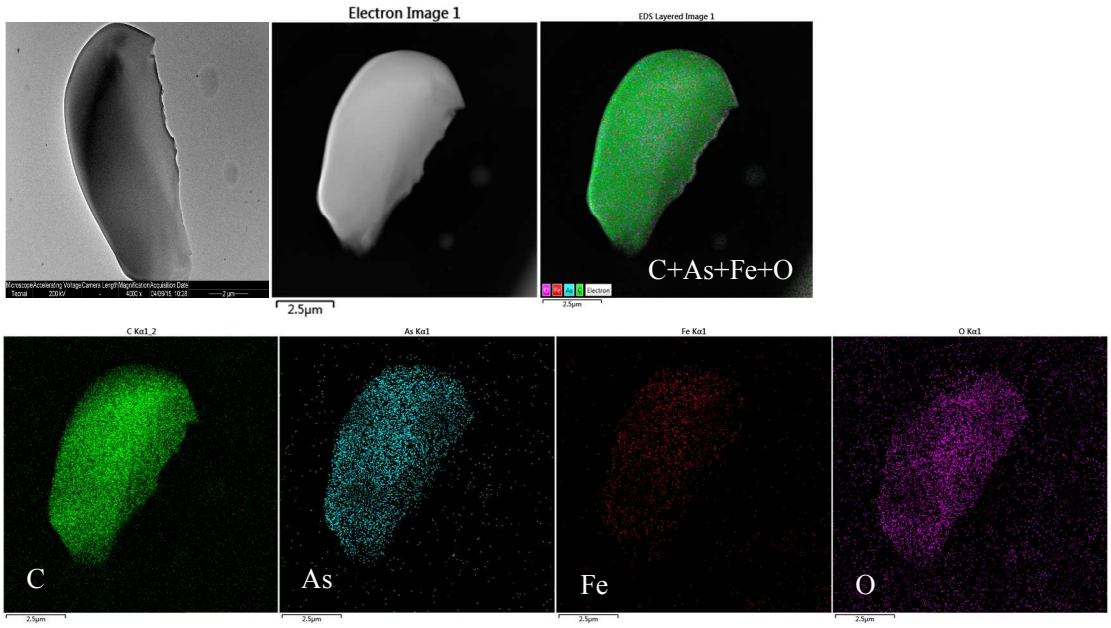

Fig. 6.

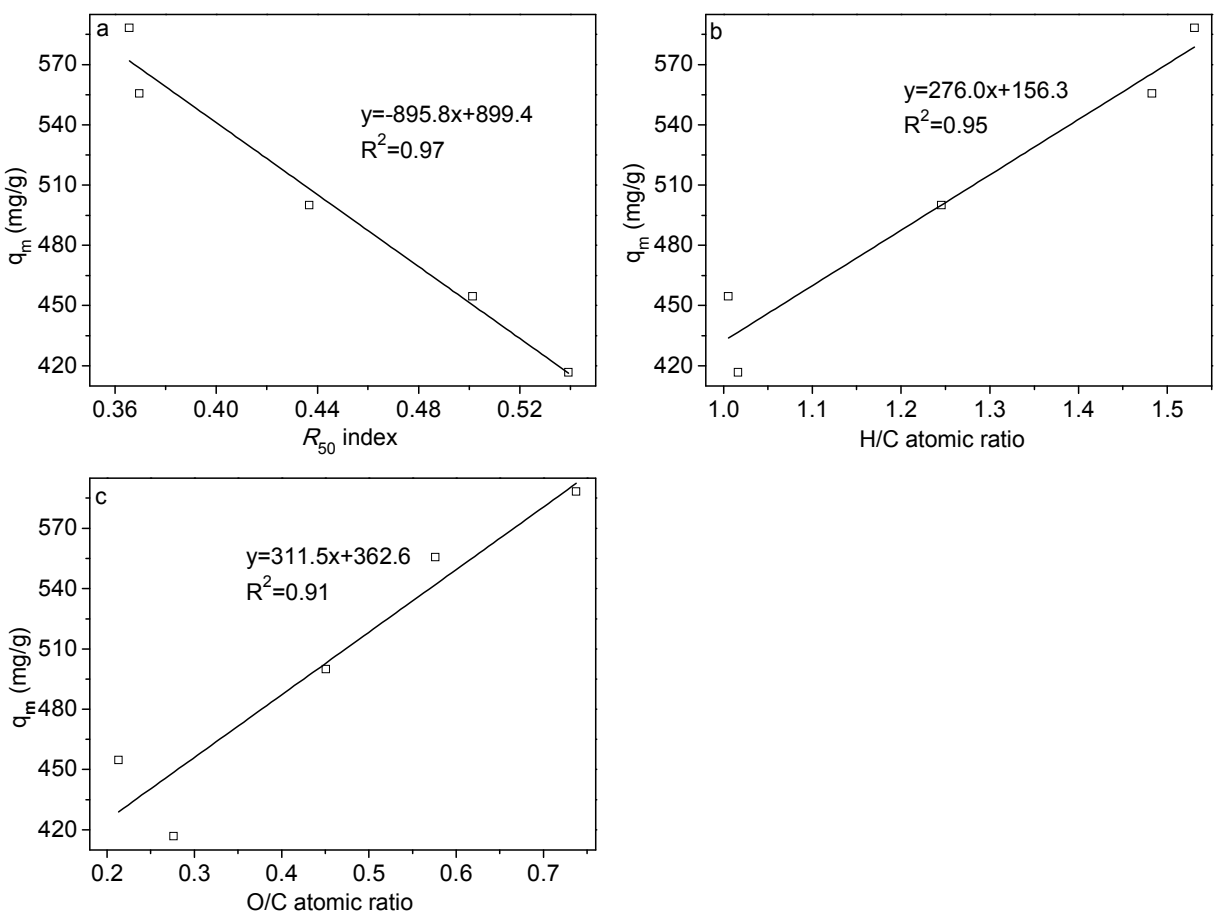

Fig. 7.

Table 1 Yields, ash, pH, atomic ratios and recalcitrance index for hydrochar samples produced under different HTC temperatures

Sample	Yield (%) [a]	Ash (%)	pH	H/C [b]	O/C [c]	R_{50} index [d]
H-160	71.2	0.05	4.10	1.53	0.74	0.36
H-200	56.3	0.12	4.10	1.48	0.58	0.37
H-240	39.5	0.16	3.63	1.25	0.45	0.44
H-270	29.9	0.42	3.99	1.01	0.21	0.50
H-300	24.9	0.52	4.12	1.02	0.28	0.54

[a] Yields are on a water-free basis. [b] H/C: atomic ratio of hydrogen to carbon. [c] O/C: atomic ratio of oxygen to carbon. [d] R_{50} index: a new thermal recalcitrance index for carbonized materials.

Table 2 Yield, surface area and pore volume for different hydrochar-derived magnetic carbon composites

Sample	Yield (%) [a]	S_{BET} [b] (m^2/g)	S_{mic} [c] (m^2/g)	S_{mic}/S_{BET} (%)	V_t [d] (cm^3/g)	V_{mic} [e] (cm^3/g)	V_{mic}/V_t (%)
MC-160	44.7	1470	1392	94.7	0.749	0.679	90.7
MC-200	47.7	1239	1180	95.2	0.642	0.586	91.2
MC-240	62.8	1142	1083	94.8	0.587	0.531	90.5
MC-270	74.5	953	828.3	86.9	0.528	0.409	77.6
MC-300	80.2	879	822	93.6	0.469	0.406	86.6

[a] Yields calculated from the magnetic carbon composite's weight to its initial hydrochar precursor's weight. [b] Brunauer-Emmett-Teller (BET) surface area calculated on the basis of N_2 adsorption data in the P/P_0 range of 0.04 to 0.3. [c] Micropore surface area calculated using the t-plot method. [d] Total pore volume determined at P/P_0 = 0.99. [e] Micropore volume calculated using the t-plot method.

247 **Table 3** Regressed pseudo-second-order kinetic parameters and Langmuir equation parameters
248 for ROX adsorption onto as-prepared magnetic carbon composites
249

	Pseudo-second-order kinetics parameters			Langmuir equation parameters		
Sample	q_e (mg/g)	k_2 (g/mg·min)	R^2	b (L/mg)	q_m (mg/g)	R^2
MC-160	515.5	13.2×10^{-4}	0.99	0.063	588.2	0.99
MC-200	502.5	10.3×10^{-4}	0.99	0.061	555.6	0.99
MC-240	427.4	17.4×10^{-4}	0.99	0.050	500.0	0.99
MC-270	421.9	5.6×10^{-4}	0.99	0.072	454.5	0.99
MC-300	381.7	3.2×10^{-4}	0.99	0.048	416.7	0.99

250
251

Graphic Abstract

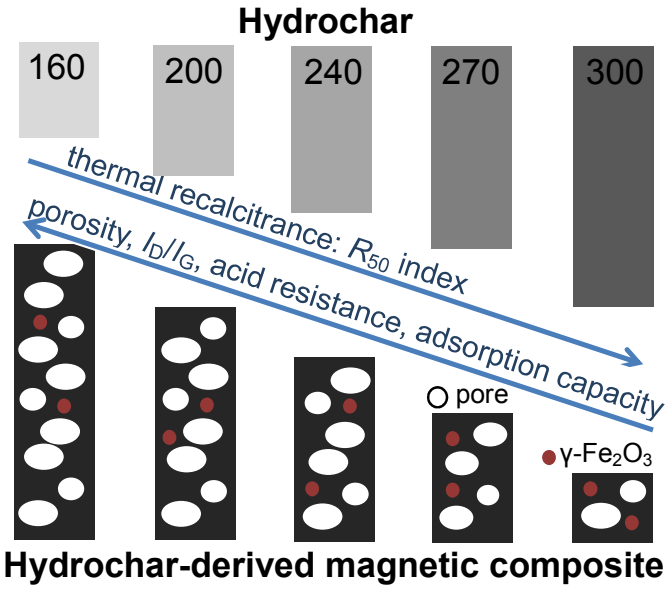

Strong linear correlations were obtained between hydrochar properties and the environmental performances of its derived magnetic carbon composites.